Research article

Journal of RAMAN SPECTROSCOPY

Received: 20 September 2011 Revised: 21 November 2011 Accepted: 22 November 2011 Published online in Wiley Online Library: 30 December 2011

(wileyonlinelibrary.com) DOI 10.1002/jrs.3145

Spectroscopy of Palaeolithic rock paintings from the Tito Bustillo and El Buxu Caves, Asturias, Spain†

Antonio Hernanz,[a]* José M. Gavira-Vallejo,[a] Juan F. Ruiz-López,[b] Santiago Martin,[c] Ángel Maroto-Valiente,[d] Rodrigo de Balbín-Behrmann,[e] Mario Menéndez[f] and Jose J. Alcolea-González[e]

Significant paintings from the Tito Bustillo (Ribadesella, Asturias) and El Buxu (Cardes, Asturias) caves, renowned archaeological sites of the Cantabrian Palaeolithic cave art, were studied by micro-Raman spectroscopy. Auxiliary techniques like infrared spectroscopy, X-ray diffraction, X-ray photoelectron spectroscopy and scanning electronic microscopy combined with energy dispersive X-ray spectrometry were also applied. Haematite (α-Fe_2O_3) of three granular sizes (<1, <10 and <30 μm) is the main red component of these paintings. Wüstite, amorphous carbon, and Mn are additional components of some pigments. Hydroxyapatite was also detected in one pictograph. Calcite, α-quartz and clay minerals are used as filler materials. Particles of anatase are present in some cases. No organic binders were detected. Considering the main components, granular size, and secondary phases with Ni and Mn in the pigments it is concluded that the ochre quarry in the Tito Bustillo cave was not used to make the pigments of the selected paintings. Two figures of this cave seem to have been painted with a similar pigment. A possible relationship between paintings of both caves is discussed. Copyright © 2011 John Wiley & Sons, Ltd.

Supporting information may be found in the online version of this article.

Keywords: Raman microscopy; SEM/EDX; XPS; pigments; prehistoric paintings

Introduction

The Cantabrian Palaeolithic cave art was discovered in 1879 in the famous Altamira cave. Many more caves have been discovered since then, so nowadays there are almost one hundred sites with Palaeolithic art recorded in the Northern area of the Iberian Peninsula. A significant part of them were included in the UNESCO World Heritage List on 2008. The Tito Bustillo (Ribadesella, Asturias) and El Buxu (Cardes, Asturias) caves are very important archaeological sites situated on the western part of the area where the Cantabrian Palaelothic art is distributed (Fig. S1). Micro-Raman spectroscopy (MRS), is a powerful tool to identify the composition of prehistoric pictorial materials,[1,2] specially when combined with auxiliary techniques.[3–6] The characterisation of the composition of the pigments, binders, substrata and accretions is essential to consider possible relationships among pictographs from both caves, potential radiocarbon dating,[7–9] and to investigate degradation processes and to advice appropriately about the conservation of these precious Palaeolithic paintings.[3–6] This work is devoted to study pictographs from the Tito Bustillo and El Buxu caves selected according to criteria of archaeological significance and pictorial similarity between motifs from both caves (Figs S2 and S3). These pictographs have been analysed by MRS and scanning electronic microscopy combined with energy dispersive X-ray spectrometry (SEM/EDX), to identify the pigment palette composition, and consequently to compare the pictorial materials used in both archaeological sites. When the Tito Bustillo cave was discovered, an ochre quarry, 'Cantera de Colorante', was found there. This is a space located at the cave entrance in the upper part of the set XI (Fig. S2). A Palaeolithic workshop to prepare the pigment was set up in this place. Blocks of ochre were extracted directly from a vein. They were placed on several adjacent rocks and they were fragmented with stone tools found *in situ*. These 'rocky platforms' and blocks in process may be observed in the cave nowadays. The great amount

* *Correspondence to: Antonio Hernanz, Departamento de Ciencias y Técnicas Fisicoquímicas, UNED, Paseo Senda del Rey 9, E-28040 Madrid, Spain. E-mail: ahernanz@ccia.uned.es*

† *This article is part of the Journal of Raman Spectroscopy special issue entitled "Raman spectroscopy in art and archaeology" edited by Juan Manuel Madariaga and Danilo Bersani.*

a *Departamento de Ciencias y Técnicas Fisicoquímicas, Facultad de Ciencias, Universidad Nacional de Educación a Distancia (UNED), Paseo Senda del Rey 9, E-28040 Madrid, Spain*

b *Departamento de Historia, Facultad de Ciencias de la Educación y Humanidades, Universidad de Castilla-La Mancha (UCLM), Avda. de los Alfares, 44, E-16071 Cuenca, Spain*

c *Departamento de Física Matemática y de Fluidos, Facultad de Ciencias, UNED, Paseo Senda del Rey, 9, E-28040 Madrid, Spain*

d *Departamento de Química Inorgánica y Química Técnica, Facultad de Ciencias, UNED, Paseo Senda del Rey 9, E-28040 Madrid, Spain*

e *Departamento de Historia I y Filosofía, Facultad de Filosofía y Letras, Universidad de Alcalá de Henares, Colegios 2, E-28801 Alcalá de Henares, Madrid, Spain*

f *Departamento de Prehistoria y Arqueología, Facultad de Geografía e Historia, UNED, Paseo Senda del Rey 7, E-28040 Madrid, Spain*

of ochre in the Cantera de Colorante and the specific work made on this material suggest a considerable production and use of this pigment. It could be exchanged in other places of the Sella Valley, as El Buxu cave. It could also be used for the paintings of the Tito Bustillo cave, and for objects and corporal decoration. This ochre outcrop have been previously studied by petrography, X-ray diffraction (XRD), SEM/EDX and inductively coupled mass spectrometry.[10–12] Complementary information on this source of pigment have been obtained in the present work by MRS, infrared (IR) spectroscopy, XRD and X-ray photoelectron spectroscopy (XPS). The results of this study can provide very interesting information on the technologies used by Palaeolithic artists, on possible relationships between the studied pictographs and the characteristics of the pigments used.

Archaeological background

Several kinds of abstract signs and large Ice Age animal figures were painted on the walls of Cantabrian caves. These pictographs were made with complex techniques using together engraving and paint. They include a large catalogue of forms, from very simple painted or carved zoomorphic outlines to polychrome animal depictions produced by the reddish and blackish pigments, scratching and exploiting the natural contours in the cave walls. The Tito Bustillo and El Buxu caves keep a well preserved complex iconography that is a good example of the variety of Palaeolithic art techniques, and therefore these caves are outstanding places to study the chemical composition of Palaeolithic paintings. They are located in the Sella River basin and the distance between them is around 12 km (Fig. S1). A hypothetical relation between the pictorial ensembles of these two caves could be established because of their nearness and some shared stylistic features. In support of this hypothesis we should mention that the functionality of these sites has been considered complementary from an archaeological point of view.[13]

The El Buxu cave was discovered on 1916. Bison, wild goats, horses and techtiforms were engraved on its walls, and painted and engraved deer. Some painted depictions were made with charcoal. One of these figures, from the XV ensemble, was ^{14}C AMS dated at 9139 ± 170 BP,[14] a result that contradicts with the more logical stylistic chronology. According to Menéndez[13] these paintings should be classified among Leroi–Gourhan's style III and the ancient style IV, i.e. between 17 000 and 14 000 BP, a hypothesis in good agreement with the results of archaeological excavations in this site.[13] However, the red signs sampled could be older.

The Tito Bustillo cave was discovered in 1968 and it is one of the jewels of the Cantabrian Palaeolithic art, maybe only exceeded by Altamira cave. Several hundreds of animal depictions and signs are preserved on its walls, with plenty of zoomorphs of different sizes, some of them masterly created in polychromy by combining simple and repeated line engravings with several colours, scrapes and washings. The Great Panel ensemble is the most remarkable of the cave, with many superimpositions that have been used to establish a reliable diachronic sequence. Here there are horses painted in different shades of black, red and purple, very likely gathered from the red and purple ochre quarries of the original entrance to the cave. The archaeological excavations, last of them directed by de Balbín-Behrmann, have identified material and graphic evidences of the whole Upper Palaeolithic, between Aurignacian and the end of the Magdalenian times, and even the Azilian time.[15] A large ^{14}C AMS dating plan of these paintings was carried out by Fortea[14] giving for the black figures of the main panel a range of dates between 12 000 and 14 000 BP, with some dates younger than 10 000 BP for the last pictorial stage. Further ^{14}C AMS dating of black figures by de Balbín-Behrmann *et al.*[15] yielded dates around 11 500 BP. These authors have also established that organic heterogeneous fillers were added to the paint. Nevertheless, the pictographs of the 'Camarín de las Vulvas' (Fig. 1) and the Antropomorphs Gallery are considered the oldest according to stylistic conventions, criterion that set them in the Aurignacian time.

Experimental

The protocol used for microsample extraction, MRS and SEM/EDX studies of prehistoric paintings has been described elsewhere.[4–6,16] Specific experimental details of this work are mentioned in the following. As stated previously, pictographs from both caves were sampled according to the criteria of archaeological interest, graphic resemblance and characteristics of the rocky surface. A specimen of pigment (size ≤ 1 mm^2) was removed from each motif. The sampled points in the Tito Bustillo and El Buxu caves are indicated in Fig. 2, and their locations in these caves are shown in Figs S2 and S3. Only microspecimens of red pigment were extracted. Three figures were sampled in the Tito Bustillo cave (TB): figure 18 from the set III in the Camarín de las Vulvas (TBCV-III-18), figure 17 from the panel XB in the main room (TBXB-17) and a red spot next to figure 95 from the panel XE in the same room (TBXE-n95), Figs 2(a)–(c). Additionally, a specimen of about 100 g from one of the ochre blocks in process (Fig. 2(d)) in the Tito Bustillo cave was removed (TBCRR). On the other side, four figures were sampled in the El Buxu cave (B): figure i from the zone C (BCi), figures A and B (samples BPA and BPB, respectively) from an area with finger dots along the passage and finally a red line (Fig. 1) from the main chamber (BSG1) (Figs 2(e)–(h)).

The MRS study of the samples was carried out with a Jobin Yvon LabRam-IR HR-800 spectrograph coupled to an Olympus BX41 microscope. The 632.8 nm line of a He/Ne laser was used for Raman excitation with a power of 695 μW (50× LWD objective) measured at the sample position. The average spectral resolution in the Raman shift range of 100–1700 cm^{-1} was 1 cm^{-1} (focal length 800 mm, grating 1800 grooves/mm, and confocal pinhole 100 μm). These conditions involved a lateral resolving power of ~5 μm (50× LWD objective lens) at the specimen. An integration time of between 2 and 30 s and up to 64 accumulations were used to achieve an acceptable signal-to-noise ratio (SNR). The linearity (sine bar linearity) of the spectrograph was adjusted using the fluorescent lamps of the lab (zero order position) and the lines at 640.22 and 837.76 nm of a Ne lamp. The confocality of the instrument was refined using the 519.97 cm^{-1} line of a silicon wafer. Wavenumber shift calibration was accomplished with 4-acetamidophenol, naphthalene and sulphur standards[17] over

Figure 1. Paintings from the Camarín de las Vulvas (Tito Bustillo Cave, TB). The white arrow indicates the TBCV-18-III sampling point.

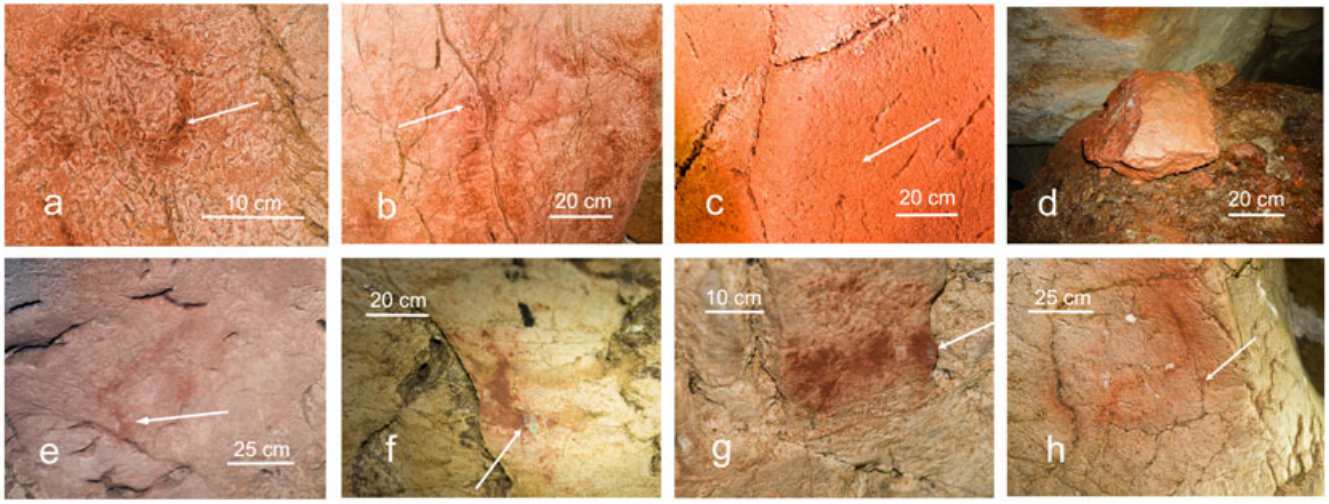

Figure 2. Pictographs from the Tito Bustillo (TB: a, b, c, d) and El Buxu (B: e, f, g, h) caves indicating the sampling points. (a) TB, Camarín de las Vulvas, set III, figure 18 (TBCV-III-18); (b) TB, main room, panel XB, figure 17 (TBXB-17); (c) TB, main room, panel XE, next to figure 95 (TBXE-n95), (d) TB, ochre block in process (TBCRR); (e) B, zone C, figure i (BCi); (f) B, passage, figure A, finger dots (BPA); (g) B, passage, figure B, finger dots (BPB); (h) B, main chamber, figure 1 (BSG1).

the range 150–3100 cm^{-1}. This resulted in a wavenumber mean deviation of $\Delta\nu_{cal}$ - $\Delta\nu_{obs}$ = 1.07 ± 0.48 cm^{-1} ($t_{Student}$ 95%). At least 30 Raman spectra were obtained from each microsample to obtain representative spectra. The abundance of each component was estimated according to the number of particles or areas in which the component has been identified. Spectral smoothing was not applied to the observed spectra. The software package GRAMS/AI v.7.00 (Thermo Electron Corporation, Salem, NH, USA) was used to assist in determining the wavenumber of the peaks and the appropriated spectral baselines.

X-ray microanalyses of the samples were carried out with an EDX spectrometer Rontec Xflash Detector 3001, Peltier-refrigerated, with the Be window removed and coupled to a Hitachi S-3000 N scanning electron microscope (Everhart-Thornley detector of secondary electrons) with an operating resolution of 3 nm.

Because of requirements from the authorities responsible for the archaeological sites, only nondestructive techniques (MRS and SEM/EDX with no Au-Pd or C coating of the samples) were applied to the microsamples removed from the pictographs. They are preserved as they were extracted for further studies in the future. However, the macrosample TBCRR was also studied by IR, XRD and XPS. It was grounded to be analysed by these techniques. A KBr pellet containing 2 mg of ground specimen into 300 mg of desiccated KBr was prepared to obtain its IR spectrum. A Bomem MB-100 FTIR spectrophotometer was used for this purpose. The 4000 to 750 cm^{-1} spectral region was recorded with a nominal resolution of 2 cm^{-1}. To obtain a good SNR, 100 interferograms have been coadded.

The XRD pattern of TBCRR was recorded in a Rayflex XRD3100 equipment using CuKα X-rays (λ = 1.54 Å) and a Ni filter. Steps of 0.01° were employed with a time of 2 s per step.

The XPS spectra were recorded with an Omicron spectrometer equipped with an EA-125 hemispherical electron multichannel analyser and unmonochromatised Mg Kα X-ray source having a radiation energy of 1253.6 eV at 150 W and a pass energy of 20 eV. The specimen was pressed into a small pellet of around 5–15 mm diameter. This pellet was mounted on the sample holder and introduced into the chamber where it was degassed for 6–8 h to achieve a dynamic vacuum below 10^{-8} Pa prior to the analysis. The resulting spectral data were analysed using the CASA XPS software and RSF database for peak fitting and Shirley background correction. The binding energy was referenced to the adventitious C 1s peak at 285 eV.

Results and discussions

The results obtained are summarised in Table 1. Haematite, α-Fe_2O_3, is the main component of the pigment used in all the studied pictographs (Figs 3(b) and (c)). This mineral is commonly used in prehistoric paintings.[1,3–6,18–21] Therefore, its spectral and morphological characteristics, additional components, secondary phases with other minerals (Fig. 4) and elements present in the paint should be considered to establish possible relationships among different pictographs or archaeological sites. Representative Raman signatures of the studied pigments are collected in Table 2. The ochre specimen TBCRR show clear differences with the rest of the pigments. The observed shift to lower wavenumber and broadening of the Raman band at 400 cm^{-1} of TBCRR indicates that this pigment contains very disordered haematite, i.e. a structural intermediate between haematite and goethite.[1] More ordered crystal structures of haematite are present in the other specimens. Additional details in the Raman signature of TBCRR, Table 2, confirm that this source of pigment differs notably from the pigments used in the studied pictographs. The spectral profile of the haematite particles from the different specimens in the region of 520–740 cm^{-1} (Fig. 5) is another indication of the possible disorder in the crystal structure of haematite. [22–26] The haematite band at ~607 cm^{-1} (E_g) appears in this region, but a new band at ~655 cm^{-1} may be observed in disordered structures. This band was assigned to magnetite or maghemite associated to haematite in ochre.[1,27] However, studies made on heating haematite assigned this band to an IR active longitudinal optical E_u mode, observable in Raman because of the change of symmetry in disordered structures.[28,29] A progressive increase of the relative intensity of the band at ~655 cm^{-1} in the 607–655 cm^{-1} doublet for the different pigments may be seen in Fig. 5. Again, TBCRR appears as the specimen containing haematite with the most disordered crystal structure.

Table 1. Results obtained from pigment specimens of significant Palaeolithic pictographs from the Tito Bustillo (TB) and El Buxu (B) caves. Components and elements in secondary phases are given in order of abundance

Specimen	Components	Granular size	Elements in secondary phases
TBCV-III-18	haematite, calcite, hydroxyapatite, clay	h.c. $\phi < 1\mu$m c.c. $\phi < 10\mu$m	K, P, Mg, S
TBXB-17	haematite, calcite, α-quartz, clay	h.c. $\phi < 10\mu$m q.c., c.c. $\phi < 50\mu$m	P, K, Ni, Mg, S
TBXE-n95	calcite, haematite, clay, α-quartz, anatase	h.c. $\phi < 10\mu$m q.c., c.c. $\phi < 50\mu$m	S, P, Ni, Mg, K
TBCRR	α-quartz, clay, calcite, haematite, anatase, a.c.	h.c. $\phi < 10\mu$m q.c., c.c. $\phi < 100\mu$m	P, Na
BCi	haematite, calcite, clay, wüstite, a.c.	h.c. $\phi < 10\mu$m c.c. $\phi < 100\mu$m	K, P, Mn
BPA	haematite, calcite, clay, α-quartz, a.c.	h.c. $\phi < 10\mu$m c.c. ϕ ~100μm q.c. $\phi < 10\mu$m	P, Ni, K, Mg
BPB	haematite, clay, wüstite, calcite	h.c. $\phi < 30\ \mu$m c.c. $\phi < 100\mu$m	K
BSG1	haematite, wüstite, calcite, clay	h.c. $\phi < 10\mu$m c.c. $\phi < 100\mu$m	Mn, K, P

a.c., amorphous carbon; c.c., calcite crystals; h.c., haematite crystals; q.c., α-quartz crystals.

The granular size of the particles, Table 1, was determined from the observed microscopic images. Some examples corresponding to the specimens BPA and BCi may be seen in the microphotographs shown in Figs S4 and S5. Haematite was processed to reach a fine granular size, i.e. less than 1 μm, in TBCV-III-18 indicating a complex technique to prepare the pigment. On the contrary, a gross type of haematite particles was used in BPB (<30 μm). An intermediate granular size, <10 μm, similar to the present in TBCRR, was used in the rest of specimens (Figs S4 and S5). Calcite particles were also detected in all specimens (Table 1 and Fig. 4(c)). This is not significant because both caves are in a karstic area. Moreover, the Cantabrian Sea and the Sella River are in close proximity to the caves and the use of molten mollusc shells to prepare the paint has been previously mentioned.[15] α-Quartz is abundant in TBCRR, but few particles were found in TBXB-17, TBXE-n95 and BPA (Fig. 4(b) and Tables 1 and 2). Wüstite, a nonstoichiometric iron oxide ($Fe_{0.84}O$–$Fe_{0.95}O$)[28] was detected in BCi, BPB and BSG1, i.e. in three pictographs from the El Buxu cave (Fig. 3(a) and Tables 1 and 2). The broad band of wüstite at 643 cm^{-1} can be well distinguished from those of magnetite and haematite at 663 and 655 cm^{-1}, respectively.[28] Some particles of anatase, TiO_2, were observed in TBCRR and TBXE-n95 (Fig. 4(d) and Tables 1 and 2). A very weak Raman band at 962 cm^{-1} appears in some spectra of TBCV-III-18 (Fig. 3(c)). This band may be assigned to hydroxyapatite, suggesting the addition of small amounts of calcined bones to the paint. This has been observed previously in other prehistoric paintings.[5] On the other hand, the broad D1 and G bands of amorphous carbon are observed at 1341 and 1582 cm^{-1}, respectively[5,18,30] in the spectra of TBCRR

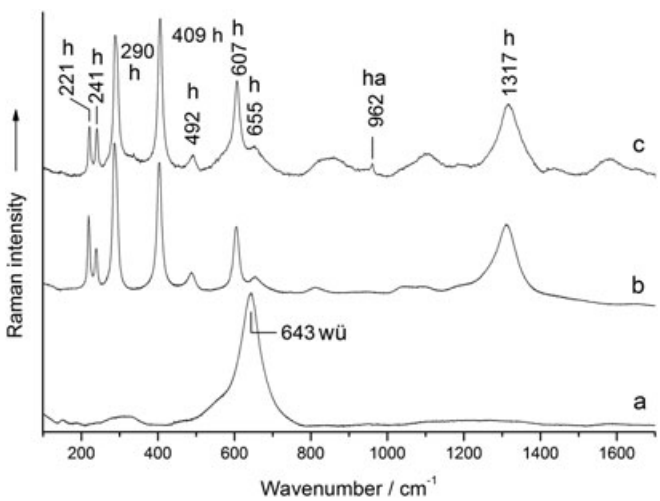

Figure 3. Raman spectra of representative points of the specimens of red pigment from the Tito Bustillo and El Buxu caves: (a) BPB, wüstite; (b) BSG1, haematite; (c) TBCV-III-18, haematite with a small amount of hydroxyapatite. Baseline correction has been applied to the spectra a and c. h, haematite; ha, hydroxyapatite; wü, wüstite.

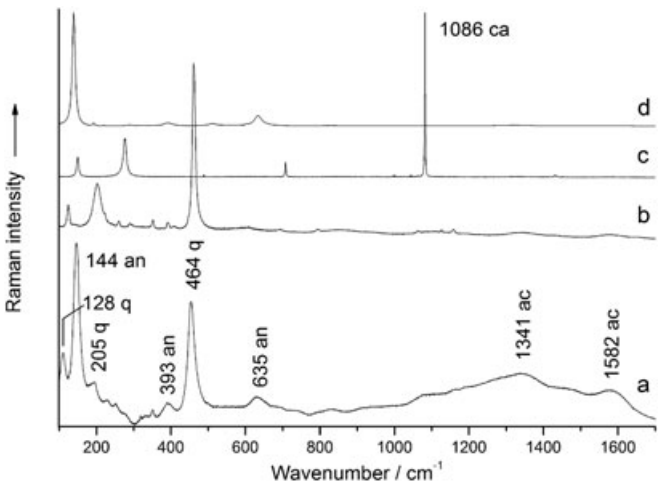

Figure 4. Raman spectra of representative points of the specimens extracted from the Tito Bustillo and El Buxu caves: (a) TBCRR, clast of red rock with α-quartz, anatase, and amorphous carbon; (b) TBXB, α-quartz; (c) BPA, calcite; and (d) TBXE, anatase. Baseline correction has been applied to the spectrum a. ac, amorphous carbon; an, anatase; ca, calcite; q, α-quartz.

Table 2. Representative Raman signatures of red pigments from the Tito Bustillo and El Buxu caves. Peaks observed in cm^{-1}. Wavenumbers between parentheses are sometimes observed

Component	Specimen							
	TBCV-III-18	TBXB-17	TBXE-n95	TBCRR	BCi	BPA	BPB	BSG1
α-Quartz	—	(124 w)	(123 w)	—	—	123 w	—	—
Anatase	—	—	(139 vs)	(140 vs)	—	—	—	—
Calcite	(151 vw)	(152 w)	(150 w)	150 w	(150 w)	—	(149 w)	(149 vvw)
Anatase	—	—	(192 vvw)	—	—	—	—	—
α-Quartz	—	(201w)	(201w)	—	—	201 w	—	—
Haematite	222 m	222 s	221 vs	218 w	221 m	221 w	220 m	220 w
—	243 w	242 w	241 vw	237 vvw	241 w	238 vw	240 w	240 w
α-Quartz	—	(262 vvw)	(260 vvw)	—	—	260 vvw	—	—
Calcite	(278 m)	(278 m)	(276 m)	276 m	(277 m)	277 m	(275 w)	—
Anatase	—	—	(289 vvw)	—	—	—	—	—
Haematite	290 vs	287 vs	287 m	286 m	289 vs	286 s	287 vs	289 s
—	295 sh	295 sh	294 sh	—	293 sh	—	293 sh	292 sh
α-Quartz	—	(351 vvw)	(351 vvw)	—	—	351 vw	—	—
—	—	(392 vvw)	(390 vvw)	—	—	390 w	—	—
Anatase	—	—	(393 vvw)	—	—	—	—	—
α-Quartz	—	(462 vs)	(460 vs)	460 vs	—	460 vs	—	—
Haematite	**409 s**	**412 s**	**412 m**	**400 m**	**407 s**	**412 s**	**407 s**	**407 s**
FWHH[a]	**13**	**13**	**12**	**21**	**14**	**14**	**15**	**14**
—	494 w	494 w	495 vw	—	492 w	—	492 vw	489 vw
Anatase	—	—	(511 vvw)	—	—	—	—	—
Haematite	**609 m**	**607 m**	**606 w**	**601 m**	**608 m**	**606 m**	**607 m**	**608 m**
Anatase	—	—	(634 vvw)	—	—	—	—	—
Wüstite	—	—	—	—	643 s	—	643 s	643 s
Haematite	656 w	657vvw	—	651 m	655 w	656 w	654 w	653 w
Calcite	(710 vvw)	(710 vw)	(708 w)	708 w	(708 vw)	708 w	(708 vw)	—
Hydroxyapatite	(960 vw)	—	—	—	—	—	—	—
Calcite	(1084 vs)	(1084 vs)	(1083 vs)	1083 vs	(1083 vs)	1082 vs	(1082 vs)	(1083 w)
α-Quartz	—	(1159 vvw)	(1158 vvw)	—	—	(1158 vvw)	—	—
Haematite	**1318 m**	**1313 m**	**1313 m**	**1305 s**	**1315 m**	**1313 m**	**1317 s**	**1314 m**
Amph. carbon	—	—	—	1341 m	1355 s	1315 s	—	—
Calcite	(1434 vvw)	(1434 vvw)	(1432 vvw)	—	(1433 vvw)	1432 vvw	1432 vvw	—
Amph. carbon	—	—	—	1582 m	1586 s	1581 m	—	—

[a]FWHH, full-width at half-height of the previous Raman band; Amph. carbon, amorphous carbon; vs, very strong; s, strong; m, medium; w, weak; vw, very weak; vvw, very very weak; sh, shoulder.

(Fig. 4(a)). Amorphous carbon was also detected in BCi and BPA (Tables 1 and 2). This disordered carbonaceous material could be due to rests of organic matter present in the red rock (specimen TBCRR), either in the minerals used to prepare the paint or an intentional addition of this material to make the paint darker (specimens BCi and BPA). An intense background of fluorescence radiation was observed in the Raman spectra of most of the specimens. The weaker background was observed in the spectra of TBCV-III-18. Clay minerals present in the samples could give rise to this fluorescence radiation.[6] Auxiliary techniques such as IR, XRD, XPS and EDX were used to enlighten this point and to obtain additional data on the specimens.

The IR spectrum of the sample TBCRR (Fig. 6) gives information on the main components present in the ochre block (Fig. 2(d)). The IR bands observed at 1425 and 875 cm^{-1} are due to the asymmetric stretching ν_3 (E_u) and out-of-plane bending ν_2 (A_{2u}) modes of calcite respectively.[31,32] The weak bands at 1799 and 2514 cm^{-1} are also due to calcite.[31] The spectral shoulders observed at 1087 and 1165 cm^{-1} are assigned to α-quartz bands, and those at 799 and 779 cm^{-1}.[33] The presence of dioctahedral phyllosilicates frequently found in clay like illite and montmorillonite[33] would explain the additional bands observed in the IR spectrum of TBCRR. The strong band at 1028 cm^{-1} may be assigned to the Si–O–(Al) antisymmetric stretching vibration of illite[33–35], and the shoulder at 914 cm^{-1} and additional contributions to the bands observed at 799 and 779 cm^{-1}. The broad absorption between 3300 and 3800 cm^{-1} with a peak at 3627 cm^{-1} can be assigned to the O–H stretching mode of these clay minerals.

The XRD pattern of TBCRR (Fig. S6) confirms that calcite and α-quartz are abundant in the red rock. Nevertheless, very weak signals at 20° and 35° (2θ) suggest the presence of illite.[36] Similarly, a very weak peak of haematite could be glimpsed at about 33° (2θ), but its SNR is so bad that the corresponding assignment has not been included in Fig. S6. Previous XRD studies on this ochre source do not detect iron oxides[10–12] indicating that the concentration of these minerals is lower than the detection limit of ~2 wt%.

The XPS peaks of K, Mg and Al observed in the spectrum of TBCRR (Fig. S7), together with those of Fe, Si and O are further indications of the existence of clay minerals like illite in the TBCRR. The peaks of Ca,

Journal of RAMAN SPECTROSCOPY

O, Fe and C support the results obtained by MRS and IR spectroscopy. A detailed examination of the spectral region of the C and K peaks (Fig. S8) shows two different C 1s peaks corresponding to the organic and inorganic carbon. The first one is due to amorphous carbon detected previously by MRS and the second one to the carbonate anion, CO_3^{2-}, of calcite.

The EDX spectrum of TBCRR (Fig. S9) shows also significant peaks of Al, K and Mg with others of Fe, Si and O. This is an additional sign of the presence of illite in TBCRR. The peak of Ti confirms the detection of anatase by MRS. A small quantity of P is also present in the specimen as indicated by the very weak peak of this element. The rest of the peaks in the EDX spectrum corroborate the results obtained previously by MRS, IR, XRD and XPS. The EDX spectra of TBCV-III-18, TBXB-17 and TBXE-n95 (Figs S10–S12) confirm also the results obtained before for the paintings from the Tito Bustillo cave. Nevertheless, it is important to note that a small amount of P and S is present in all of them. Using MRS, hydroxyapatite was detected only in TBCV-III-18. Weak peaks of Ni are observed in the EDX spectra of TBXB-17 and TBXE-n95, but not in the spectrum of TBCV-III-18. These results emphasise the clear differences between TBCV-III-18 and the other two specimens. Moreover, α-quartz was not detected in TBCV-III-18, the granular size of the haematite particles is different in this specimen, Table 1, and peaks of anatase, Ti and Na have not been observed. Therefore, we can establish that the pigment used in the figure TBCV-III-18 was not obtained from the ochre quarry (TBCRR), and this pigment is noticeably different from those used in the pictographs TBXB-17 and TBXE-n95. Even though particles of anatase were hardly detected in TBXE-n95 and a very weak Ti peak appears in the corresponding EDX spectrum (Fig. S12), the results obtained (Fig. 5 and Tables 1 and 2) indicate that these last two figures could have been painted with the same type of pigment. The presence of Ni in the corresponding specimens indicates that another source than the ochre quarry (TBCRR) was used to make the pigment for these two pictographs. A weak peak of Ni may also be observed in the EDX spectrum of BPA from the El Buxu cave

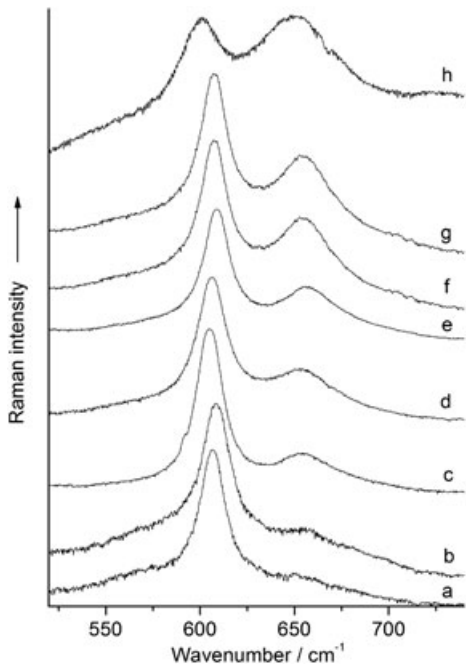

Figure 5. Representative Raman spectra in the range 520–740 cm^{-1} of haematite particles from the specimens: (a) BSG1; (b) TBXB; (c) TBXE; (d) BPB; (e) TBCV; (f) BPA; (g) BCi; and (h) TBCRR.

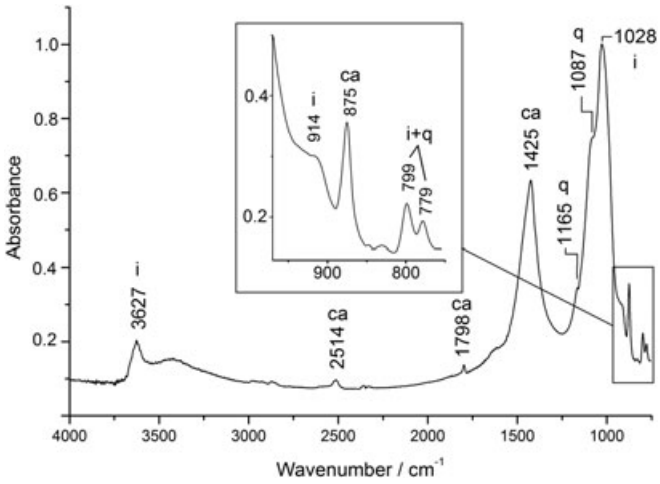

Figure 6. IR spectrum of the specimen TBCRR from the quarry of red rock in the Tito Bustillo cave. KBr pellet containing with 2 mg of sample in 300 mg of KBr. ca, calcite; q, α-quartz; i, illite.

(Fig. S13). Despite evident similarities of this pigment with TBXB-17 and TBXE-n95 (Tables 1 and 2), the different contribution of haematite disordered structures (Fig. 5) and the presence of amorphous carbon as an additional component in BPA make it difficult to establish a clear relationship between the pictograph BPA of the El Buxu cave with the TBXB-17 and TBXE-n95 pictographs of the Tito Bustillo cave. Peaks of Mn appear in the EDX spectra of BSG1 and BCi (Figs S14, S15 and S18). Both pigments of the El Buxu cave have analogous characteristics (Tables 1 and 2), but they have spectral profiles rather different in the 520–740 cm^{-1} spectral region (Figs 5(a) and (g)). Haematite disordered structures are significant in BCi but they are not relevant in BSG1. Moreover, residual particles of amorphous carbon were only detected in BCi. Therefore, a definite relationship between both pigments of the El Buxu cave cannot be established. On the other side, Mn has not been encountered in the pigments of the Tito Bustillo cave. Hence, BCi and BSG1 pigments from the El Buxu cave cannot be related with those of the Tito Bustillo cave. The EDX spectrum of BPB (Fig. S19) does not show peaks of Ni and Mn, wüstite was detected in BPB by MRS and the granular size of the hematite particles observed in this pigment are considerably larger than those of the rest of pigments. Thus, BPB pigment is different from the other pigments used in the El Buxu and the Tito Bustillo caves. Finally, the presence of amorphous carbon, wüstite and Mn in the pigments of the El Buxu cave (Tables 1 and 2) could tentatively be interpreted as an attempt to make them darker.

Conclusions

Micro-Raman spectroscopy complemented with IR, XRD, XPS and SEM/EDX is a very efficient set of techniques to characterise Palaeolithic pigments. Haematite, α-Fe_2O_3, pulverized to reach three granular sizes (<1, <10 and <30 μm) is the dominant red component used to paint the selected pictographs from the Tito Bustillo and El Buxu caves. The finest granular size was discovered in TBCV-III-18, i.e. the most complex technique to enhance the quality of the pigment. Hydroxyapatite has also been detected in this pigment, suggesting the addition of small amounts of calcined bones. Wüstite, amorphous carbon and Mn have been found as supplementary and darker components in pigments (BCi, BPB and

BSG1) from the El Buxu cave. Calcite, α-quartz and clay minerals (illite mainly) accompany the previous pigment components as filler materials. Some particles of anatase have been detected in TBXE-n95 and TBCRR. No sign of organic binders has been observed. Considering the main components, granular size, contents of haematite disordered structures and secondary phases with Ni and Mn it is concluded that none of the pigments extracted from the Tito Bustillo and El Buxu caves were prepared from the ochre quarry of this cave. The pigment used to paint the figure TBCV-III-18 is different from the pigment used in TBXB-17 and TBXE-n95, whereas these two figures seem to have been painted with an analogous pigment. Figure BPB was painted with a pigment manifestly different from the other pigments used in the El Buxu and Tito Bustillo caves, while the pigments used in the BCi and BSG1 pictographs have some similarities. The only possible relation between the pigments of both caves has been found in the figures BPA from the El Buxu cave and the pair of figures TBXB-17 and TBXE-n95 from the Tito Bustillo cave. Nevertheless, a clear relationship between these pigments from both caves has not been feasible because of different contributions of haematite disordered structures, and the presence of amorphous carbon as an additional component in BPA.

Acknowledgements

We gratefully acknowledge financial support from the European Regional Development Fund (ERDF). We also thank the Consejería de Cultura del Principado de Asturias for permission to take photographs and samples of the paintings and substrata of the archaeological sites. Three referees and Editor Philippe Colomban offered comments that significantly improved the manuscript.

Supporting information

Supporting information may be found in the online version of this article.

References

[1] F. Ospitali, D. C. Smith, M. Lorblanchet, *J. Raman Spectrosc.* **2006**, *37*, 1063.
[2] H. G. M. Edwards, D. W. Farwell, *J. Raman Spectrosc.* **2008**, *39*, 985.
[3] A. Hernanz, M. Mas, B. Gavilán, B. Hernández, *J. Raman Spectrosc.* **2006**, *37*, 492.
[4] A. Hernanz, J. M. Gavira-Vallejo, J. F. Ruiz-López, *J. Raman Spectrosc.* **2006**, *37*, 1054.
[5] A. Hernanz, J. M. Gavira-Vallejo, J. F. Ruiz-López, H. G. M. Edwards, *J. Raman Spectrosc.* **2008**, *39*, 972.
[6] A. Hernanz, J. F. Ruiz-López, J. M. Gavira-Vallejo, S. Martín, E. Gavrilenko, *J. Raman Spectrosc.* **2010**, *41*, 1104.
[7] M. W. Rowe, *Rock Art Res.* **2004**, *21*, 145.
[8] J. F. Ruiz, M. Mas, A. Hernanz, M. W. Rowe, K. L. Steelman, J. M. Gavira, *Int. Newsl. Rock Art (INORA)* **2006**, *46*, 1.
[9] M. W. Rowe, *Anal. Chem.* **2009**, *81*, 1728.
[10] E. Iriarte, A. Foyo, M. A. Sánchez, C. Tomillo, *Archaeometry* **2009**, *51*, 231.
[11] J. V. Navarro Gascón, M. L. Gómez González, in *El Arte Prehistórico desde los Inicios del Siglo XXI. Primer Symposium Internacional de Arte Prehistórico de Ribadesella* (Eds: R. de Balbín-Behrmann, P. Bueno-Ramírez), Asociación Cultural Amigos Ribadesella, Ribadesella, Spain, **2003**, pp. 161–172.
[12] J. V. Navarro Gascón, in *El Arte Prehistórico desde los Inicios del Siglo XXI. Primer Symposium Internacional de Arte Prehistórico de Ribadesella* (Eds: R. de Balbín-Behrmann, P. Bueno-Ramírez), Asociación Cultural Amigos Ribadesella, Ribadesella, Spain, **2003**, pp. 173–184.
[13] M. Menéndez, in *Excavaciones Arqueológicas en Asturias (1995–1998)*, Principado de Asturias, Oviedo, Spain, **1999**, *4*, pp. 69–73.
[14] F. J. Fortea, *Bulletin de la Société Préhistorique Ariège-Pyrénées* **2002**, *LVII*, 7.
[15] R. Balbín-Behrmann, J. J. Alcolea-González, M. A. González-Perea, in *El Arte Prehistórico desde los Inicios del Siglo XXI. Primer Symposium Internacional de Arte Prehistórico de Ribadesella* (Eds: R. de Balbín-Behrmann, P. Bueno-Ramírez), Asociación Cultural Amigos Ribadesella, Ribadesella, Spain, **2003**, pp. 91–151 and pp. 173–184.
[16] A. Hernanz, J. M. Gavira-Vallejo, J. F. Ruiz-López, *J. Optoelectron. Adv. Mater.* **2007**, *9*, 512.
[17] ASTM Subcommittee on Raman Spectroscopy. Raman Shift Frequency Standards: McCreery Group Summary (ASTM E 1840). American Society for Testing Materials: Philadelphia, PA; http://www.chem.ualberta.ca/~mccreery/raman.html (last accessed November **2011**).
[18] D. C. Smith, M. Bouchard, M. Lorblanchet, *J. Raman Spectrosc.* **1999**, *30*, 347.
[19] L. C. Prinsloo, W. Barnard, I. Meiklejohn, K. Hall, *J. Raman Spectrosc.* **2008**, *39*, 646.
[20] A. Hernanz, J. F. Ruiz-López, J. M. Gavira-Vallejo, E. Gavrilenko, S. Martín Fernández, in *Rock Chemistry* (Eds: B. Macias, F. Guajardo), Nova Science Publishers, New York, **2010**, pp. 81–102.
[21] A. Tournié, L. C. Prinsloo, C. Paris, P. Colomban, B. Smith, *J. Raman Spectrosc.* **2011**, *42*, 399.
[22] F. Froment, A. Tournié, P. Colomban, *J. Raman Spectrosc.* **2008**, *39*, 560.
[23] D. Bersani, P. P. Lottici, A. Montenero, *J. Raman Spectrosc.* **1999**, *30*, 355.
[24] J. Wang, W. B. White, J. H. Adair, *J. Am. Ceram. Soc.* **2005**, *88*, 3449.
[25] I. V. Chernyshova, M. F. Hochella, A. S. Madden, *Phys. Chem. Chem. Phys.* **2007**, *9*, 1736.
[26] A. Zoppi, C. Lofrumento, E. M. Castellucci, P. Sciau, *J. Raman Spectrosc.* **2008**, *39*, 40.
[27] D. Bikiaris, S. Daniilia, O. Katsimbiri, E. Pavlidou, A. P. Moutsatsou, V. Chryssoulakis, *Spectrochim. Acta A* **1999**, *56*, 3.
[28] D. L. A. de Faria, S. Venâncio Silva, M. T. de Oliveira, *J. Raman Spectrosc.* **1997**, *28*, 873.
[29] C. Lofrumento, M. Ricci, L. Bachechi, D. De Feo, E. M. Castelluci, *J. Raman Spectrosc.* **2011**. DOI 10.1002/jrs.3096
[30] O. Beyssac, B. Goff´e, J. P. Petitet, E. Froigneaux, M. Moreau, J. N. Rouzaud, *Spectrochim. Acta, Part A* **2003**, *59*, 2267.
[31] G. C. Jones, B. Jackson, *Infrared Transmission Spectra of Carbonate Minerals*, Chapman & Hall, London, UK, **1993**.
[32] W. B. White, in *The Infrared Spectra of Minerals* (Ed: V. C. Farmer), Mineralogical Society of London, London, UK, **1974**, pp. 227–240.
[33] H. H. W. Moenke, in *The Infrared Spectra of Minerals* (Ed: V. C. Farmer), Mineralogical Society of London, London, UK, **1974**, pp. 365–369.
[34] IRUG Spectral Database Edition 2000. NCPTT, USA. http://www.irug.org/ed2k/spectra.asp?file=IMP00071.DX (last accessed November **2011**).
[35] Mineral Spectroscopy Server, Caltech, Pasadena California, USA. http://minerals.gps.caltech.edu/FILES/Infrared_MIR/Minerals_From_JK/illite.txt (last accessed November **2011**).
[36] E. Daniels, S. Altaner, *Am. Mineral.* **1990**, *75*, 825.

Spectroscopy of Palaeolithic Rock Paintings from the Tito Bustillo and El Buxu Caves, Asturias, Spain.

Antonio Hernanz,[1]* José M. Gavira-Vallejo[1], Juan F. Ruiz-López[2], Santiago Martin,[3] Ángel Maroto-Valiente[4], Rodrigo de Balbín-Behrmann[5], Mario Menéndez[6] and Jose J. Alcolea-González[5]

[1]Departamento de Ciencias y Técnicas Fisicoquímicas, Facultad de Ciencias, Universidad Nacional de Educación a Distancia (UNED), Paseo Senda del Rey 9, E-28040 Madrid, Spain.

[2]Departamento de Historia, Facultad de Ciencias de la Educación y Humanidades, Universidad de Castilla-La Mancha (UCLM), Avda. de los Alfares, 44, E-16071 Cuenca, Spain.

[3] Departamento de Física Matemática y de Fluidos, Facultad de Ciencias, UNED, Paseo Senda del Rey, 9, E-28040 Madrid, Spain.

[4]Departamento de Química Inorgánica y Química Técnica, Facultad de Ciencias, UNED, Paseo Senda del Rey 9, E-28040 Madrid (Spain).

[5]Universidad de Alcalá de Henares, Departamento de Historia I y Filosofía, Facultad de Filosofía y Letras, Colegios 2, E-28801 Alcalá de Henares, Madrid (Spain).

[6]Departamento de Prehistoria y Arqueología, Facultad de Geografía e Historia, UNED, Paseo Senda del Rey 7, E-28040 Madrid (Spain).

*corresponding author
tel +34 91 3987377
Fax +34 91 3986697
ahernanz@ccia.uned.es

Supplementary Material for Review

Fig. S1. Location of Tito Bustillo and El Buxu caves in the Iberian Peninsula.

Fig. S2. Tito Bustillo cave plan. Sampled points are indicated.

Fig. S3. El Buxu cave plan. Sampled points are indicated.

Fig. S4. Microphotograph of the sample of pigment BPA with 50x LWD objective. Red particles of haematite may be observed on a calcite microcrystal.

Fig. S5. Microphotograph of the sample of pigment BCi with 50x LWD objective. Red particles of haematite may be observed on a calcite microcrystals.

Fig. S6. XRD pattern of TBCRR showing peaks of calcite (▼) and α-quartz (●). Very weak peaks at 20^0 and 35^0 could be associated to illite.

Fig. S7. XPS spectrum of TBCRR. The C 1s - K 2p region is expanded in Fig. S6.

Fig. S8. XPS spectrum of TBCRR, expansion of the C 1s - K 2p region. C 1s peaks from amorphous carbon and carbonate anion are differentiated.

Fig. S9. EDX spectrum of TBCRR from the Tito Bustillo cave. Ordinate axis expanded to appreciate peaks of the less abundant elements.

Fig. S10. EDX spectrum of the pigment TBCV-III-18 from the Tito Bustillo cave. (*) Peak due to copper from the holder used.

Fig. S11. EDX spectrum of the pigment TBXB-17 from the Tito Bustillo cave. Ordinate expansion on top. (*) Peaks due to copper from the holder used.

Fig. S12. EDX spectrum of the pigment TBXE-n95 from the Tito Bustillo cave. Ordinate axis expanded to appreciate peaks of the less abundant elements. (*) Peak due to copper from the holder used.

Fig. S13. EDX spectrum of the pigment BPA from the El Buxu cave. Ordinate axis expanded to appreciate peaks of the less abundant elements. (*) Peak due to copper from the holder used.

Fig. S14. EDX spectrum of the pigment BSG1 from the El Buxu cave. Ordinate axis expanded to appreciate peaks of the less abundant elements. (*) Peaks due to copper from the holder used.

Fig. S15. EDX spectrum of the pigment BCi from the El Buxu cave. Ordinate axis expanded to appreciate peaks of the less abundant elements. (*) Peak due to copper from the holder used.

Fig. S16. SEM image of the pigment BSG1 from the El Buxu cave. Au-Pd coating has not been applied to avoid sample contamination. Overexposed areas appear for this reason.

Fig. S17. Mapping of Fe in the area of the SEM image of Fig. S14. Pigment BSG1 from the El Buxu cave.

Fig. S18. Mapping of Mn in the area of the SEM image of Fig. S14. Pigment BSG1 from the El Buxu cave .

Fig. S19. EDX spectrum of the pigment BPB from the El Buxu cave. Ordinate axis expanded to appreciate peaks of the less abundant elements. (*) Peak due to copper from the holder used.

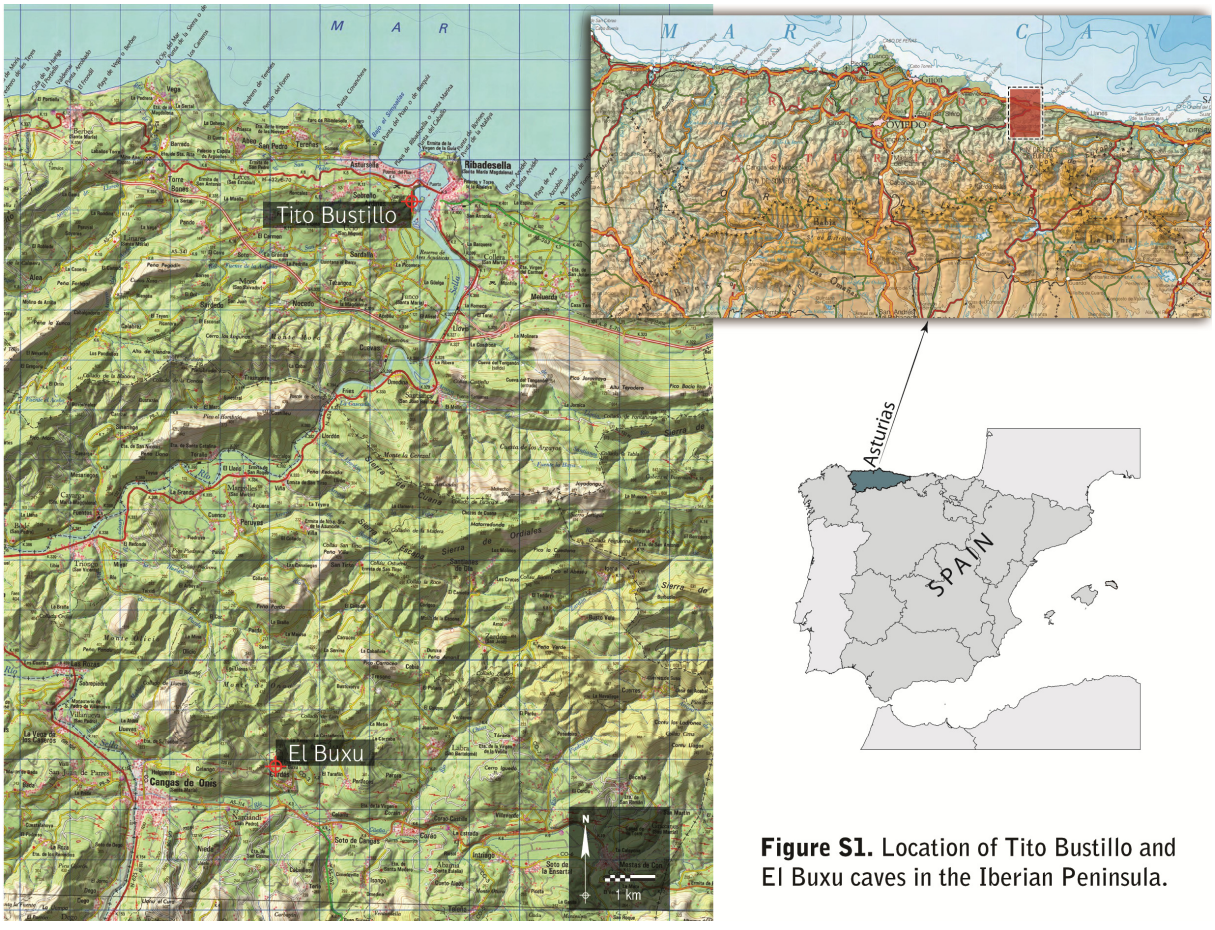

Figure S1. Location of Tito Bustillo and El Buxu caves in the Iberian Peninsula.

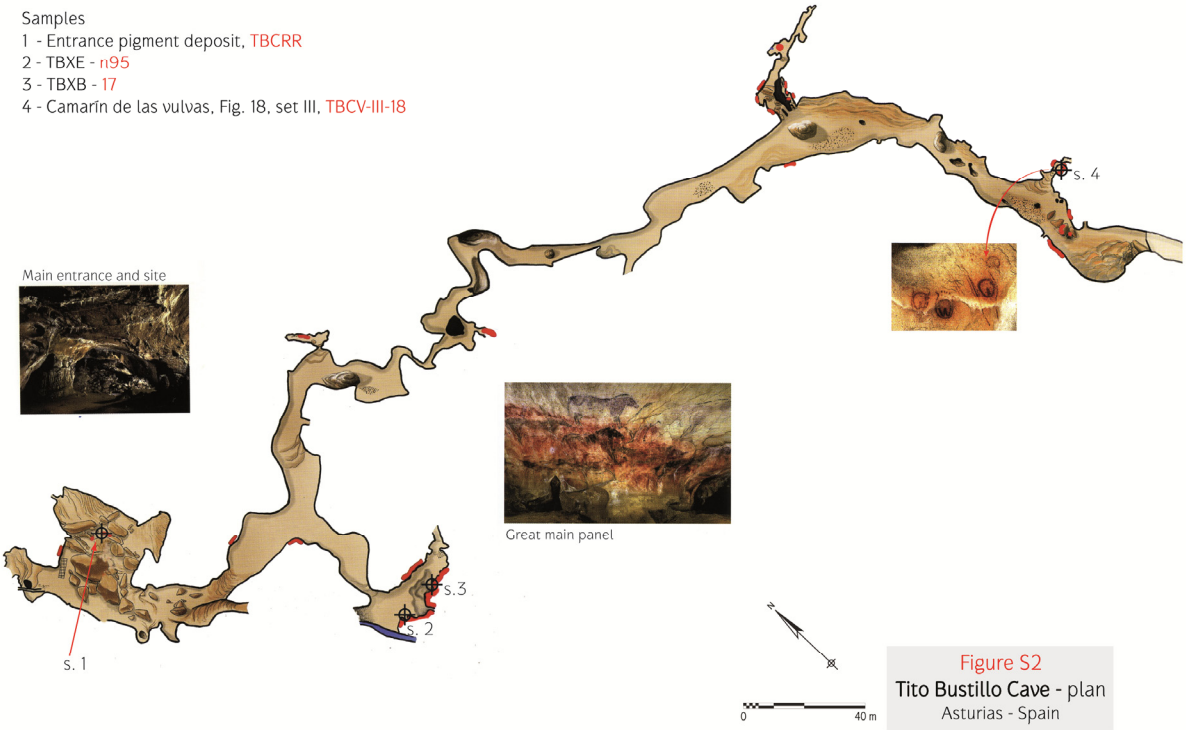

Figure S2
Tito Bustillo Cave - plan
Asturias - Spain

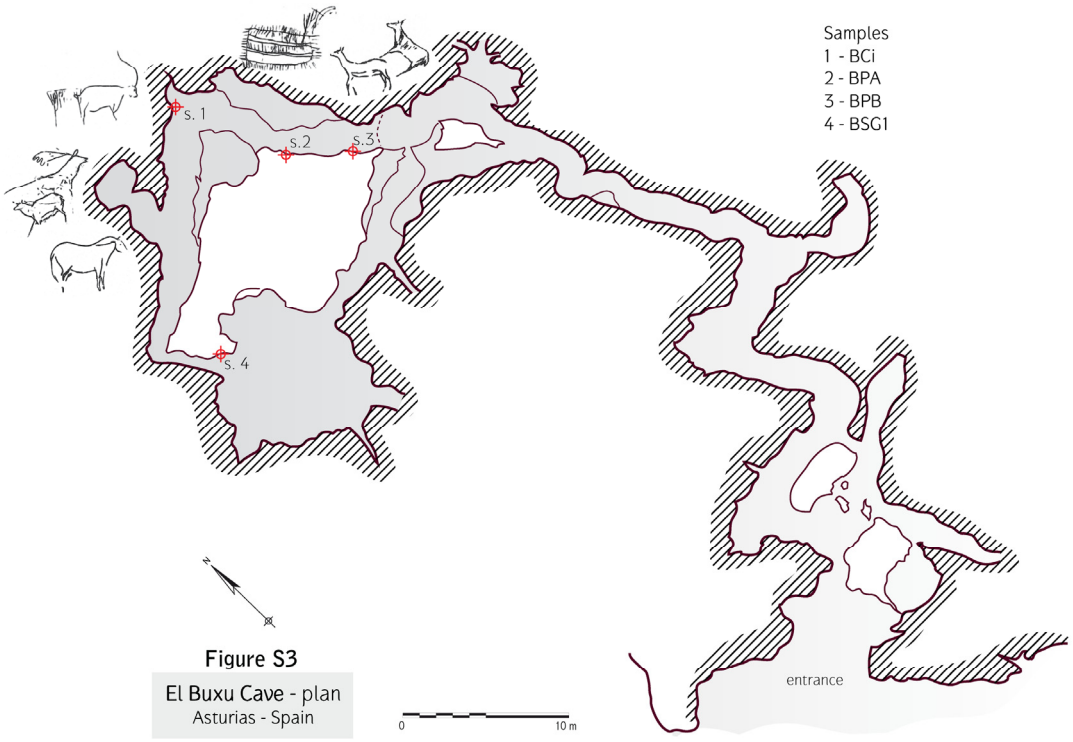

Figure S3
El Buxu Cave - plan
Asturias - Spain

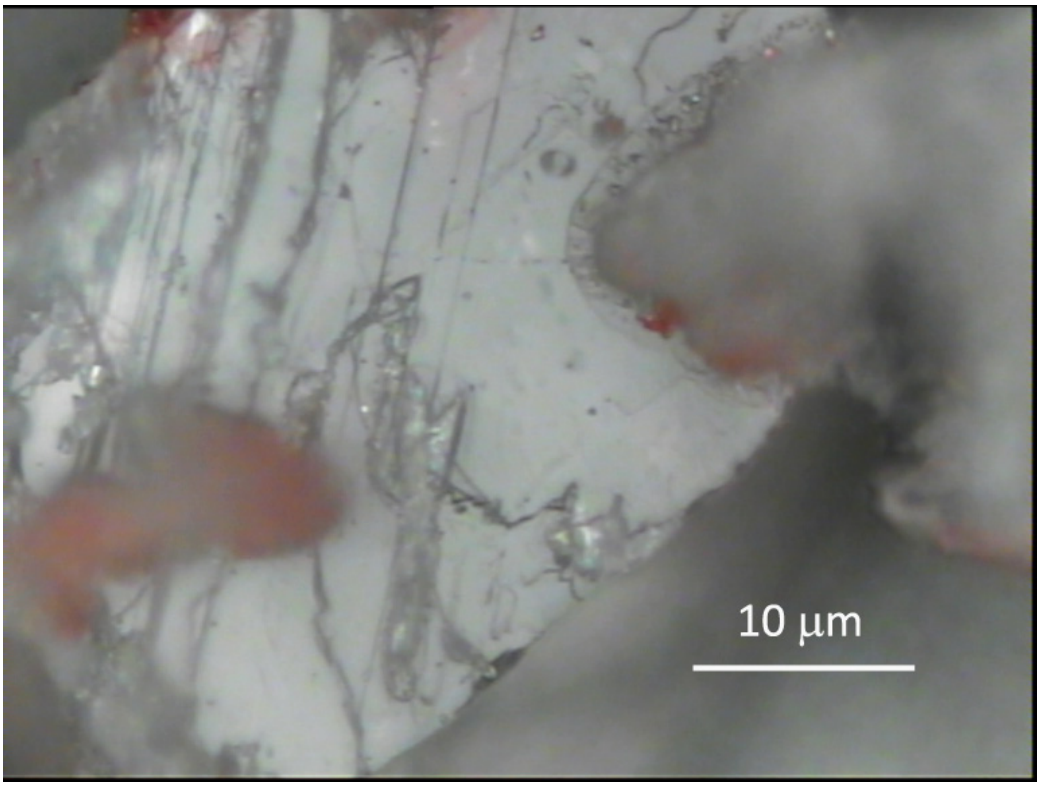

Figure S4. Microphotograph of the specimen of pigment BPA with 50x LWD objective. Red particles of haematite may be observed on a calcite microcrystal.

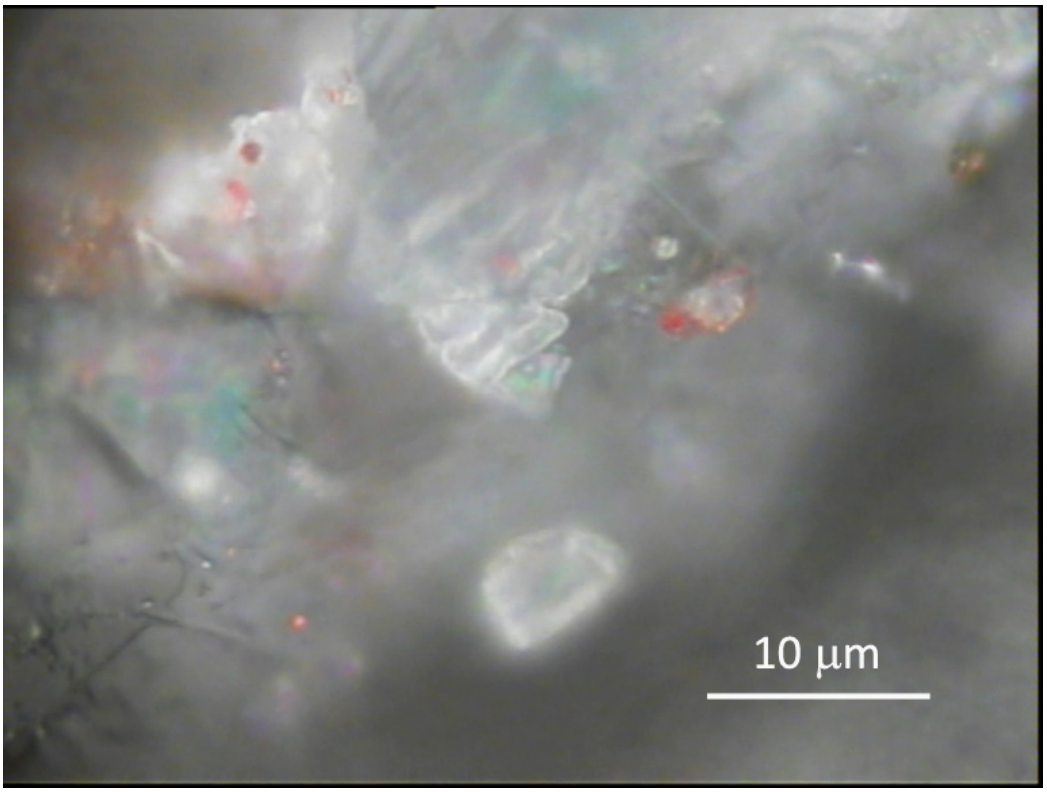

Figure S5. Microphotograph of the sample of pigment BCi with 50x LWD objective. Red particles of haematite may be observed on calcite microcrystals.

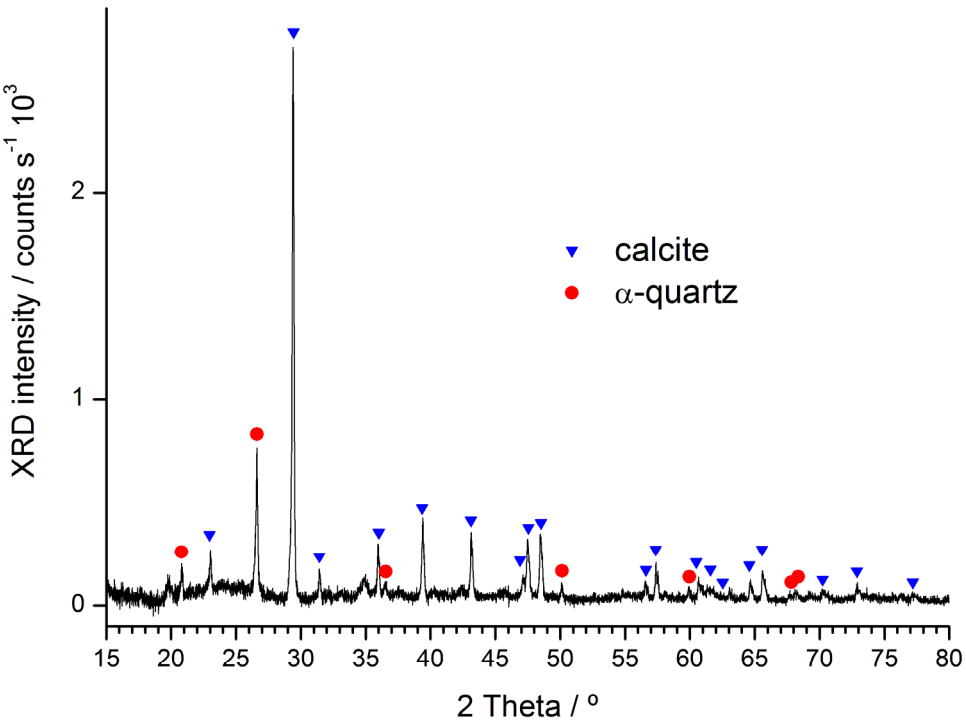

Figure S6. XRD pattern of TBCRR showing peaks of calcite (▼) and α-quartz (●). Very weak peaks at 20^0 and 35^0 could be associated to illite.

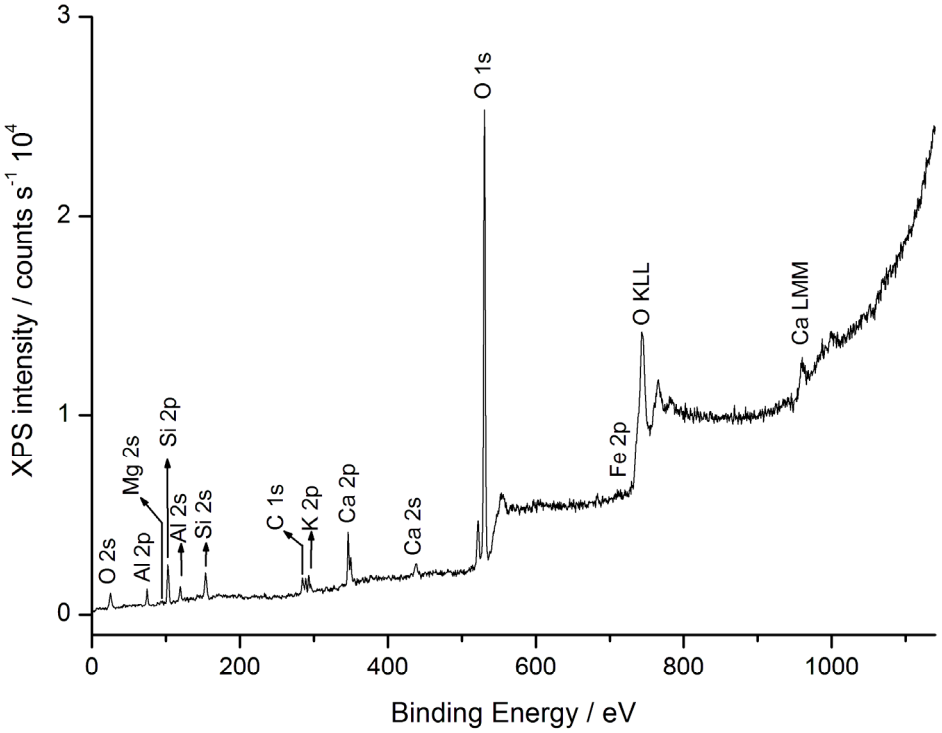

Figure S7. XPS spectrum of TBCRR. The C 1s - K 2p region is expanded in Fig. S6.

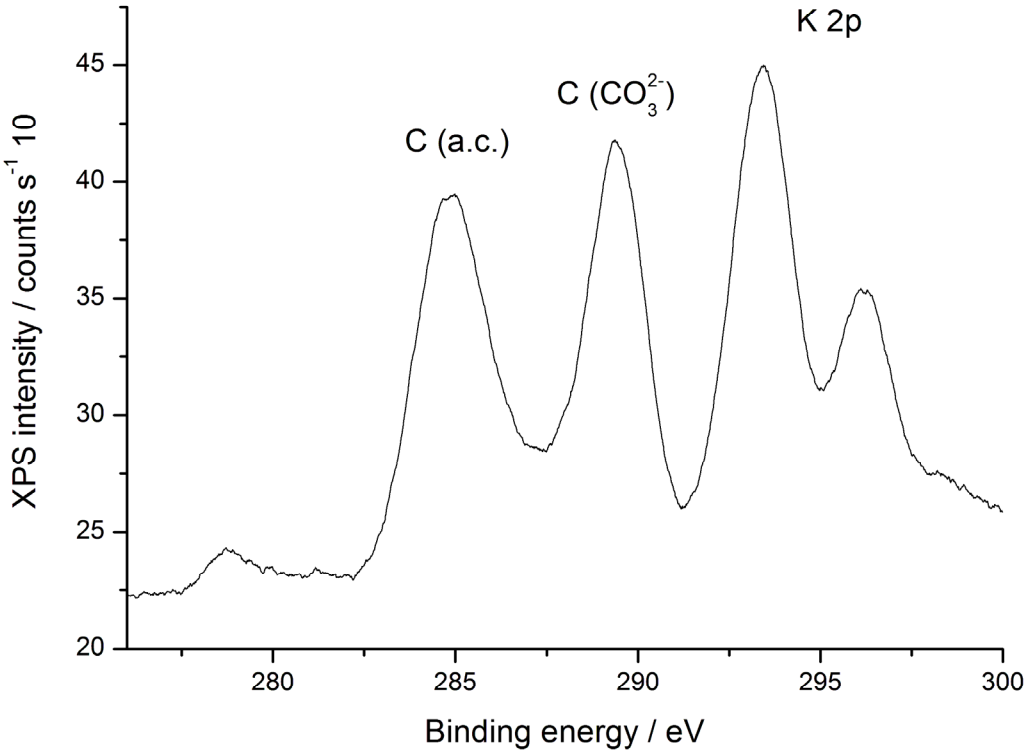

Figure S8. XPS spectrum of TBCRR, expansion of the C 1s - K 2p region. C 1s peaks from amorphous carbon and carbonate anion are differentiated

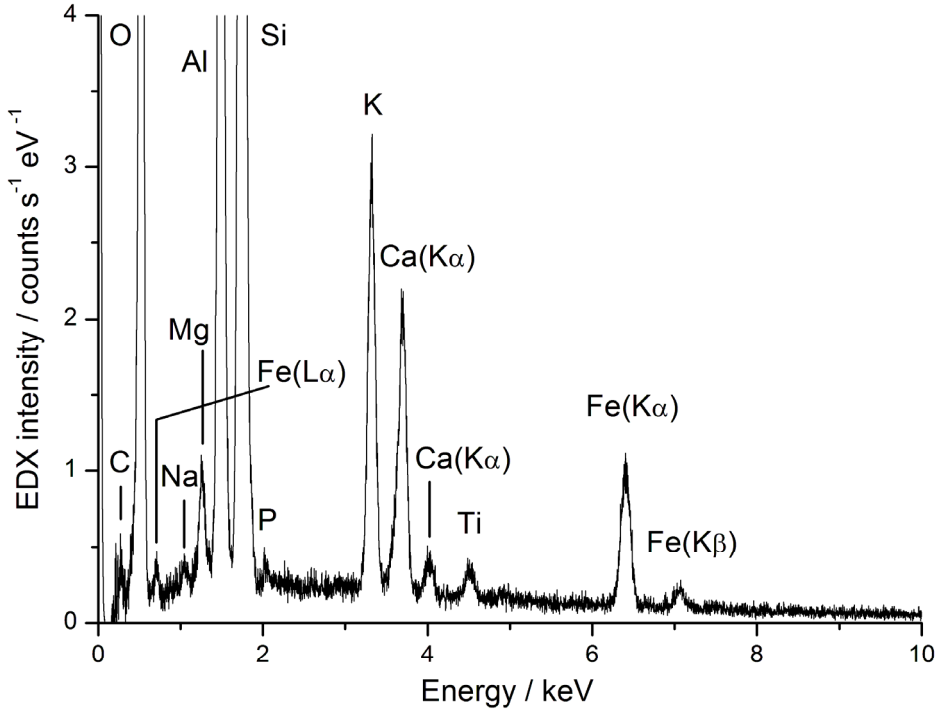

Figure S9. EDX spectrum of TBCRR from the Tito Bustillo cave. Ordinate axis expanded to appreciate peaks of the less abundant elements.

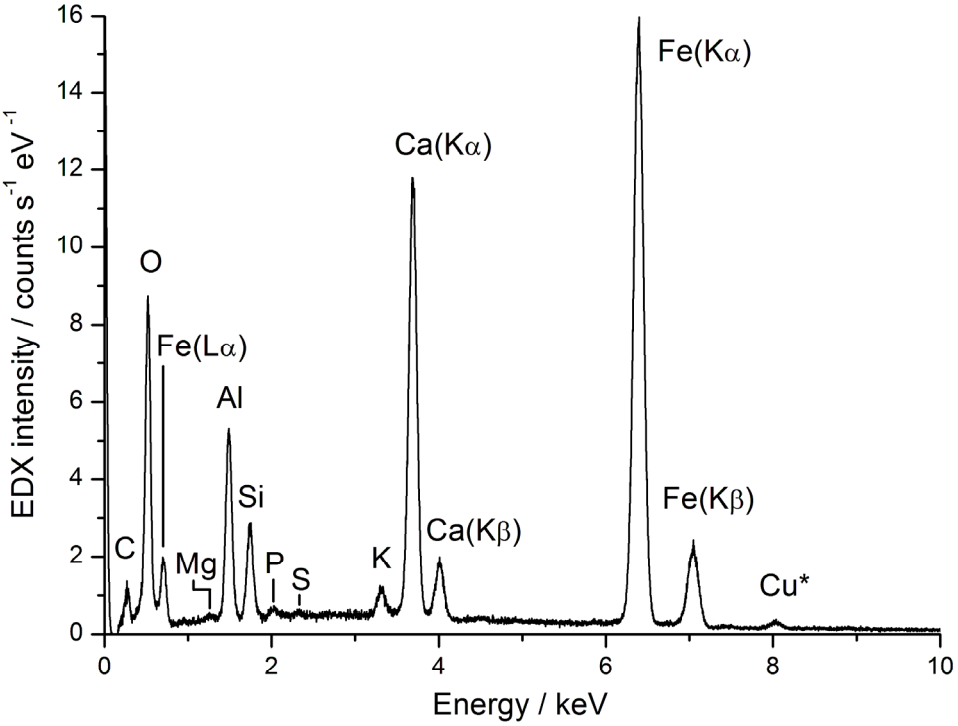

Fig. S10. EDX spectrum of the pigment TBCV-III-18 from the Tito Bustillo cave. (*) Peak due to copper from the holder used.

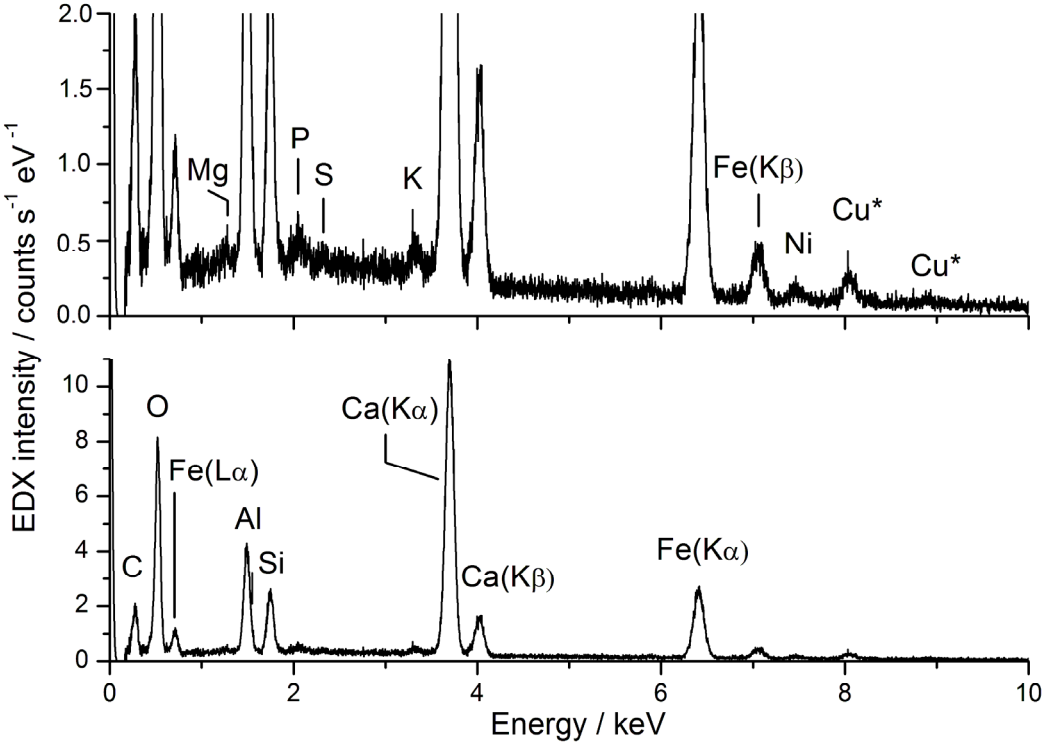

Fig. S11. EDX spectrum of the pigment TBXB-17 from the Tito Bustillo cave. Ordinate expansion on top. (*) Peaks due to copper from the holder used.

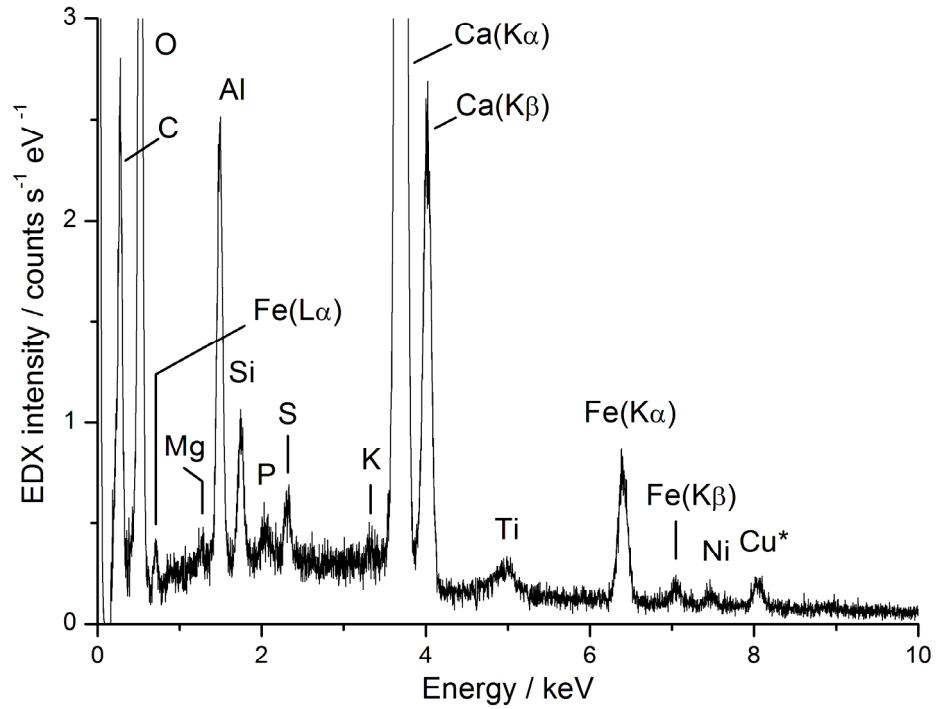

Figure S12. EDX spectrum of the pigment TBXE-n95 from the Tito Bustillo cave. Ordinate axis expanded to appreciate peaks of the less abundant elements. (*) Peak due to copper from the holder used.

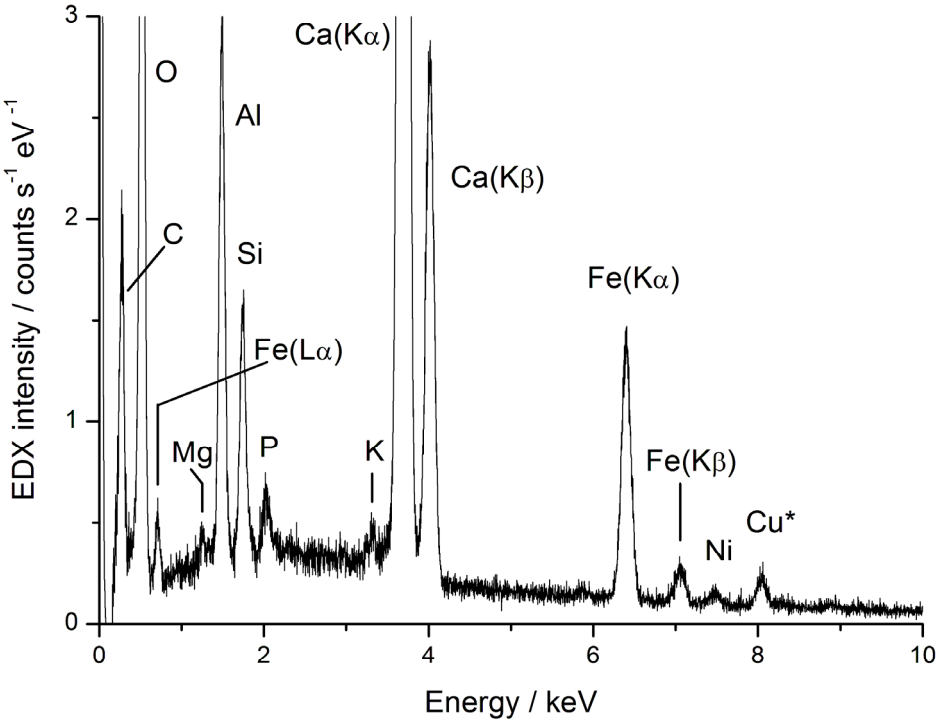

Figure S13. EDX spectrum of the pigment BPA from the El Buxu cave. Ordinate axis expanded to appreciate peaks of the less abundant elements. (*) Peak due to copper from the holder used.

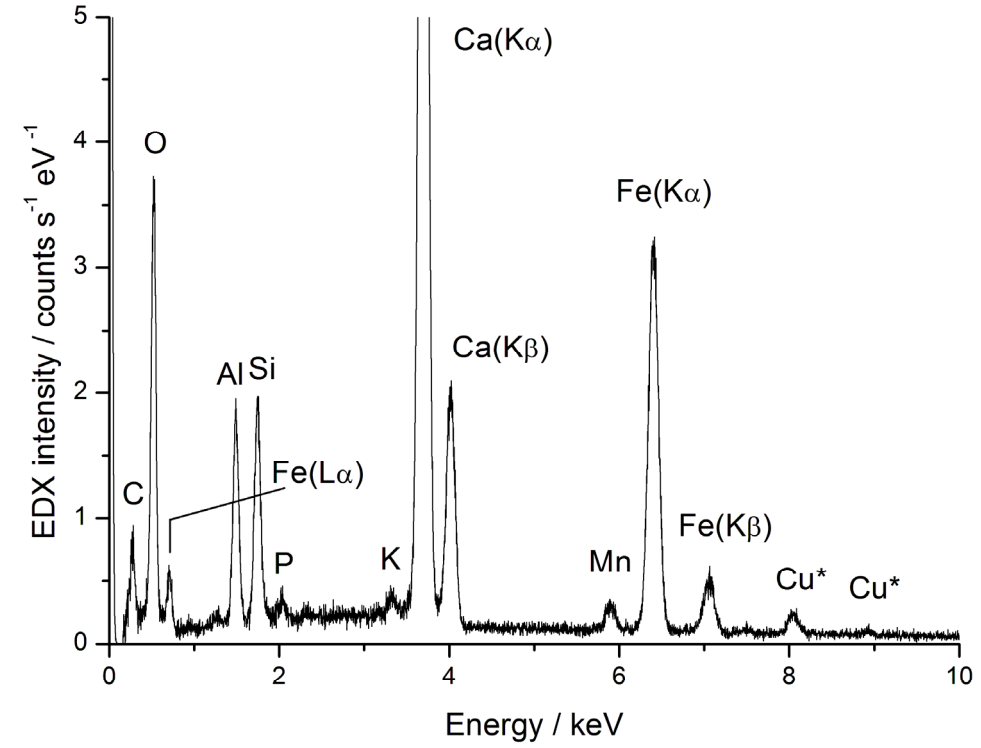

Figure S14. EDX spectrum of the pigment BSG1 from the El Buxu cave. Ordinate axis expanded to appreciate peaks of the less abundant elements. (*) Peaks due to copper from the holder used.

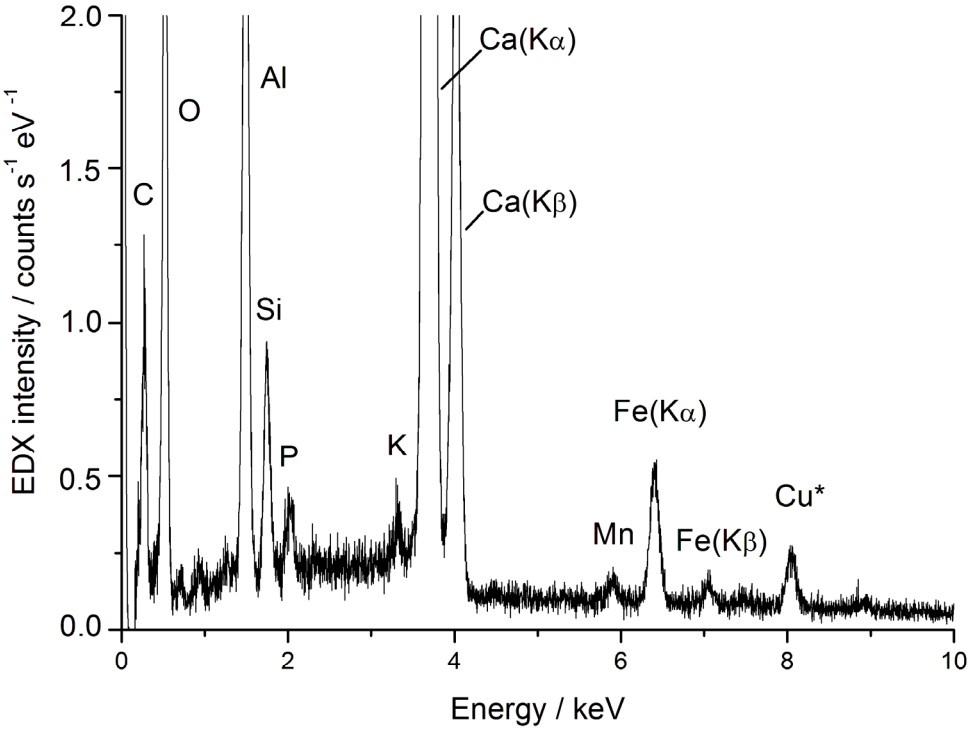

Figure S15. EDX spectrum of the pigment BCi from the El Buxu cave. Ordinate axis expanded to appreciate peaks of the less abundant elements. (*) Peak due to copper from the holder used.

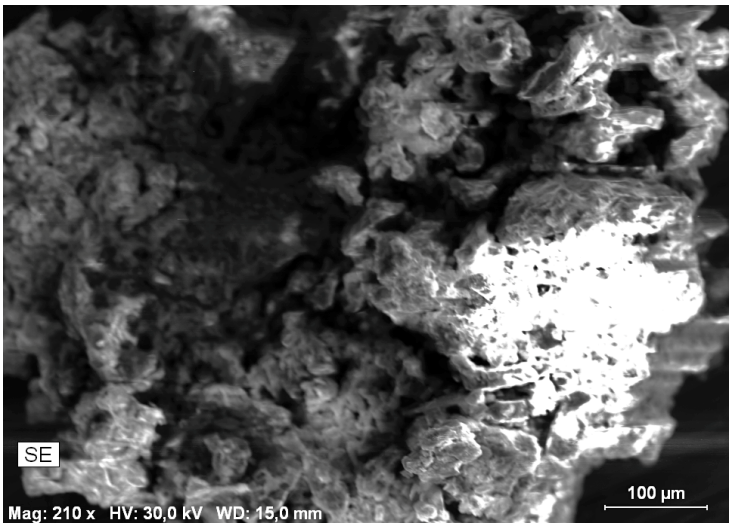

Figure S16. SEM image of the pigment BSG1 from the El Buxu cave. Au-Pd coating has not been applied to avoid sample contamination. Overexposed areas appear for this reason.

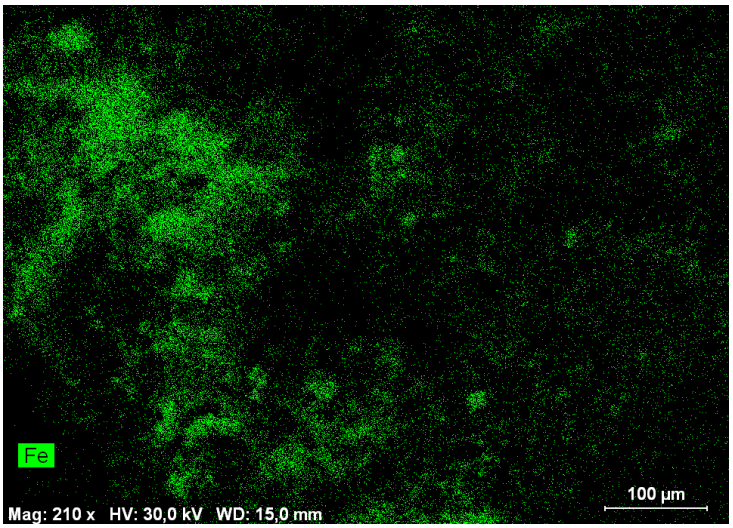

Figure S17. Mapping of Fe in the area of the SEM image of Fig. S7. Pigment BSG1 from the El Buxu cave.

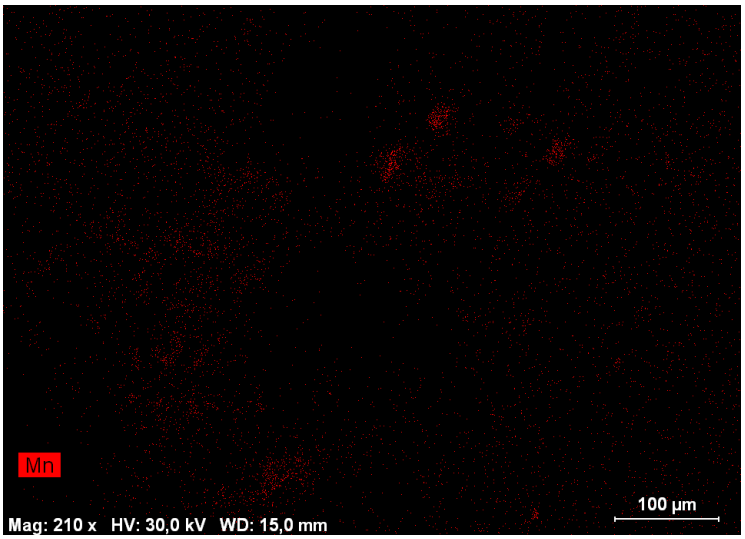

Figure S18. Mapping of Mn in the area of the SEM image of Fig. S7. Pigment BSG1 from the El Buxu cave.

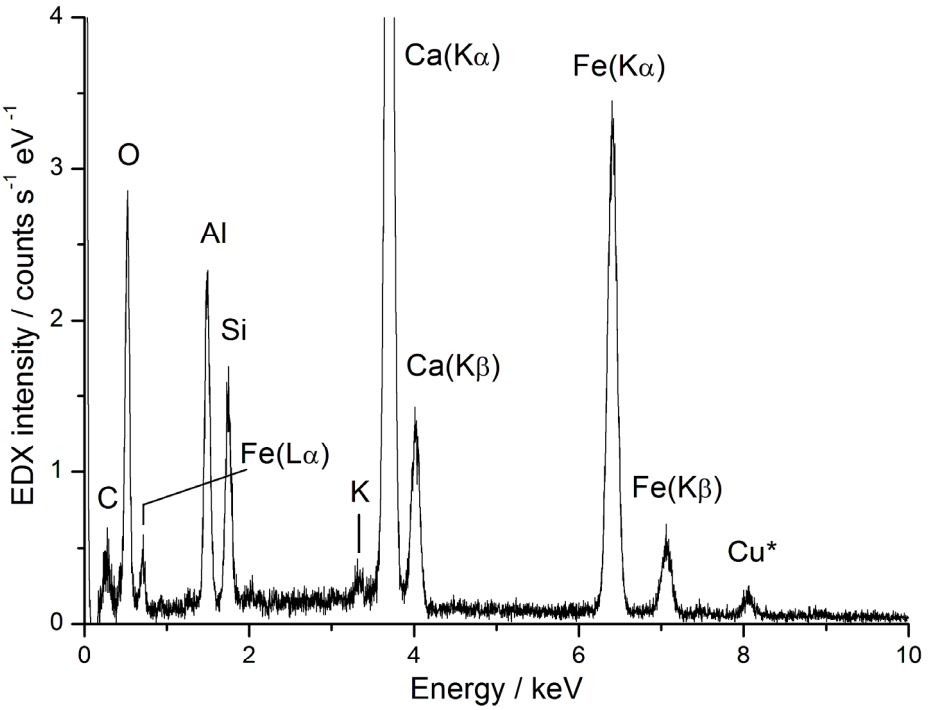

Figure S19. EDX spectrum of the pigment BPB from the El Buxu cave. Ordinate axis expanded to appreciate peaks of the less abundant elements. (*) Peak due to copper from the holder used.